Polarimetric Measurements in a Severe Hailstorm

D. S. ZRNIĆ

National Severe Storms Laboratory, Norman, Oklahoma

V. N. BRINGI

Department of Electrical Engineering, Colorado State University, Fort Collins, Colorado

N. BALAKRISHNAN

Department of Aerospace Engineering, Indian Institute of Science, Bangalore, India

K. AYDIN

Communications and Space Sciences Laboratory, The Pennsylvania State University, University Park, Pennsylvania

V. CHANDRASEKAR AND J. HUBBERT

Department of Electrical Engineering, Colorado State University, Fort Collins, Colorado

(Manuscript received 16 November 1992, in final form 15 February 1993)

ABSTRACT

This study explores the utility of polarimetric measurements for discriminating between hydrometeor types with the emphasis on (a) hail detection and discrimination of its size, (b) measurement of heavy precipitation, (c) identification and quantification of mixed-phase hydrometeors, and (d) discrimination of ice forms. In particular, we examine the specific differential phase, the backscatter differential phase, the correlation coefficient between vertically and horizontally polarized waves, and the differential reflectivity, collected from a storm at close range. Three range–height cross sections are analyzed together with complementary data from a prototype WSR-88D radar. The case is interesting because it demonstrates the complementary nature of these polarimetric measurands. Self-consistency among them allows qualitative and some quantitative discrimination between hydrometeors.

1. Introduction

There are four polarimetric weather radars operating at a 10-cm wavelength (S band) in the United States (Bringi and Hendry 1990). All four polarimetric radars use switching between vertical and horizontal polarization. This technique is simple yet effective for discrimination between types of hydrometeors. Analysis of polarimetric data has already produced significant insights into the evolution of hydrometeors in storms (Wakimoto and Bringi 1988) and promises to improve quantitative estimation of precipitation (Aydin et al. 1990b; Chandrasekar et al. 1990). Until very recently only two parameters, differential reflectivity Z_{DR} (Seliga and Bringi 1976), and linear depolarization ratio were measured with radars that transmit two linear orthogonal polarizations. Specific differential phase (also referred to as differential propagation phase constant), K_{DP}, can also be estimated, if the Doppler radar is able to measure Z_{DR}. We define K_{DP} as the difference between propagation phase constants for horizontally and vertically polarized waves.[1] Seliga and Bringi (1978) first proposed K_{DP} for use with the reflectivity factor to estimate two parameters (concentration and exponent) of exponential drop size distributions. It has been exploited by Sachidananda and Zrnić (1987), Steinhorn and Zrnić (1988), and Balakrishnan and Zrnić (1990a) to estimate rainfall with a single parameter relationship (i.e., rain rate is a function of K_{DP}) and also to infer the presence of mixed-phase precipitation. The specific differential phase K_{DP} has a unique property that allows discrimination between statistically isotropic and anisotropic hydrometeors (such as be-

Corresponding author address: Dr. Dušan S. Zrnić, NOAA/NSSL, Doppler Radar and Remote Sensing Research Group, 1313 Halley Circle, Norman, OK 73069.

[1] This is two times smaller than the definition in some previous work (e.g., Sachidananda and Zrnić 1987), where K_{DP} was for a two-way propagation path.

tween hailstones and raindrops). In the most efficient practical scheme to estimate Z_{DR} and the mean Doppler velocity one must account for the differential phase ϕ_{DP} (Sachidananda and Zrnić 1989). This optimum scheme can make polarization measurements compatible with Doppler measurements. It is only a small step from ϕ_{DP} to K_{DP}; thus, the differential propagation phase constant is essentially free. In the Mie regime of scattering, ϕ_{DP} contains contributions from the backscatter differential phase, δ, which can be estimated by filtering ϕ_{DP} data in range (Hubbert et al. 1991, 1992). Modeling of backscattering demonstrates that δ changes sign over a narrow range of hydrometeor sizes (1–3 cm, dependent on refractive index) and thus could add diagnostic value to the other polarimetric measurands.

Another variable that can be estimated with a polarimetric radar is the correlation coefficient between horizontally (H) and vertically (V) polarized echoes, $|\rho_{hv}(0)|$ (denoted as ρ_{hv} from here on). The correlation coefficient depends on the orientation and shape of the hydrometeors. Heuristic arguments suggest that it could be used to gauge hail size.

It is our contention that together all of these polarization measurands may provide a better diagnosis of hydrometeor types than is possible by any one alone. We also expect that measurement of precipitation amounts should be more accurate if these variables are used together. This is because the phase of precipitation could be determined and thus would not confuse interpretation of the measurement; furthermore, for some precipitation types, polarimetric variables have redundancy that can be used to check self-consistency of data.

An experiment was conducted at the end of May and beginning of June 1989 in Norman, Oklahoma. The experiment was part of the Cooperative Oklahoma P-3 Studies Program; the goals of this smaller part of the experiment were to

1) explore the use of Z, Z_{DR}, K_{DP}, δ, and ρ_{hv} (a) to quantify liquid water in a mixture of rain and hail and (b) to determine hail size;
2) relate hail and mixed-phase evolution to the kinematic fields in storms.

Time series data (i.e., individual echo voltages) were collected from several storms with the National Severe Storms Laboratory (NSSL) polarimetric radar, but only one storm (on 6 June) had high reflectivity (>60 dBZ) suitable for hail studies. Unfortunately, lightning hit the radar and damaged the polarization circuit about 30 min after the data collection began. Because the storms moved rapidly and the time series data require long collection times, we were not able to obtain evolutionary information. Yet we obtained snapshots of polarimetric measurands from a hailstorm at a range of 40 km. This is the first time that simultaneous measurements of all of these polarimetric variables were made at such close range in a hailstorm; three interesting cross sections through the high-reflectivity core were obtained and are discussed in this paper. Data from the prototype WSR-88D radar were also recorded, and are used to describe the storm evolution and to support the interpretation of polarimetric measurements.

2. Physical bases for interpretation of measurements

One important thrust of this paper is to explore the diagnostic applications of polarimetric variables as far as various types and sizes of hydrometeors are concerned. We present here the physical justification for five simple hypotheses that are relevant to this problem. The first states that in a mixture of rain and hail, K_{DP} is almost entirely influenced by rain (Balakrishnan and Zrnić 1990a). The second hypothesis is that ρ_{hv} decreases with increasing hail size and thus could perhaps be used to infer maximum hail diameters (Balakrishnan and Zrnić 1990b). The third is that ρ_{hv} of mixed-phase hydrometeors (e.g., bottom of the melting layer) has a depression (Zrnić et al. 1992). The fourth hypothesis suggests that large reflectivity with differential reflectivity lower than −0.5 dB indicates hail with diameters mainly in the range of 2–4 cm (Aydin et al. 1990a; Balakrishnan and Zrnić 1990b). The fifth is that backscatter differential phase can be used to infer some sizes of hydrometeors. We show data and model results that seem to confirm these hypotheses.

Besides separating rain from hail in a mixture, polarization measurements may allow quantification of hail size. One method uses partitions of the Z_H, Z_{DR} plane to establish presence of hail (Aydin et al. 1986), and the Z_H values to gauge size (Lipschutz et al. 1986). But because both concentration and size determine the reflectivity factor, the estimated size is not reliable. We propose an alternate approach that is based on three physical premises.

The first premise is the observation (List 1985) that large hailstones (4–10 cm in diameter) are roughly irregular, with small or large protuberances. That is to say, hailstones do not obey fractal laws, so the protuberance to diameter ratio is not constant but may increase with size. Although this is not always the case, when true, it will result in a noticeable decrease of ρ_{hv}. It can be shown that the correlation coefficient for monodispersed Rayleigh scatterers with random Gaussian protuberances depends on the rms value of the protuberance σ_D and the diameter D of a sphere with volume equal to the hailstone (Balakrishnan and Zrnić 1990b). Theory has shown that a σ_D/D of 0.1 may reduce the correlation to 0.92.

The second premise is rooted in the fact that below the melting level there will be rain mixed with hail. The distribution of sizes, shapes, canting angles, and phase shift upon scattering from hydrometeors consisting of a rain and hail mixture broadens with increasing hail size, thus decreasing the correlation.

The third premise is that as the diameter of spongy or water-coated hailstones increases beyond 4 cm, rapid oscillations occur in Z_{DR} due to Mie scattering (Longtin et al. 1987; Aydin and Zhao 1990), which would tend to decrease the correlation.

Several recent observations suggest that negative minima of differential reflectivity are collocated or very close to the maxima of reflectivity. Husson and Pointin (1989) recorded negative Z_{DR} and have measured, with hail pads, maximum sizes of 2.3 cm. The relevant data from these investigators shows definite negative correlation between Z and Z_{DR}. A similar finding was reported by Illingworth et al. (1987). Bringi et al. (1986b) also report negative differential reflectivity and attribute it to vertically oriented hail (i.e., the larger dimension vertically oriented). These observations and their own measurements coupled with detailed modeling of backscatter lead Balakrishnan and Zrnić (1990b) to speculate that hail with diameters larger than about 2 cm would produce Z_{DR} values in the neighborhood of -1 dB. Aydin et al. (1990a) used measurements from a Colorado hailstorm and model computations (Aydin and Zhao 1990) to suggest that hail sizes between 1.2 and 4 cm may produce Z_{DR} values of -0.5 dB or less. Crude models of vertically oriented hail qualitatively reproduce some of the reported results, but sophisticated aerodynamic modeling is required to understand the physical reasons that lead to the observed backscattering properties.

Oblateness of hail is not simply related to size as is oblateness of raindrops. Yet there are indications that larger hail is more oblate and has axis ratios (i.e., ratio of smallest to largest dimension) between 0.6 and 0.8, as reported by Knight (1986). This result and the observations that larger hail seems to be vertically oriented while falling may be related. Physical considerations by List (1985) suggest that rotation about the minor axis and slight precession about the horizontal is one possible stable mode for hail fall. This is consistent with observations that oblate spheroidal hail has homogeneous layers that are thickest at the equator and thinnest at the poles. Thus, during the growth stage such hailstones have spent most of the time in a position that offers favorable growth to the equatorial region. The fact that the thickness of layers at the equator is fairly uniform suggests that these hailstones gyrate during growth and, if large enough, they probably continue to fall in this mode below the melting level. Furthermore, beyond the embryo stage the basic spheroidal symmetry is not changed by the growth (which is primarily from accretion of a unidirectional flux of droplets), implying an equal exposure of symmetrically equivalent surface points [any two circles about the minor axis and equidistant from the plane of major axes, Kry and List (1974)].

Other shapes of hailstones are conical (to 20-mm size) and ellipsoidal (10–50 mm), often with small lobes along the shortest axis (List 1985); the elongation

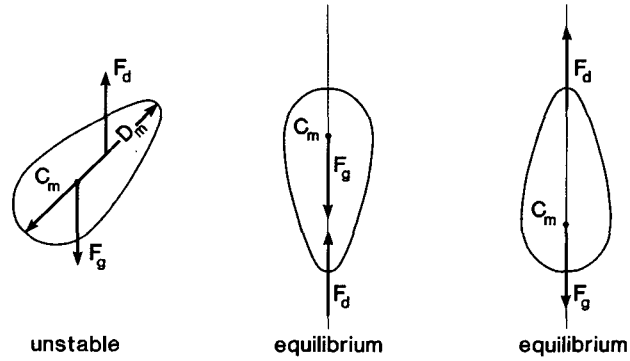

FIG. 1. Orientation of an egg- (conical) shaped hailstone in free fall. The center of gravity force $\mathbf{F}_g$ and the center of drag force $\mathbf{F}_d$ are $\mathbf{C}_g$ and $\mathbf{C}_d$.

of these hailstones is larger for larger sizes (Knight 1986), and the orientation in fall could be with the major axis vertical. This is because an equilibrium orientation of a solid body falling in a fluid is such that the drag force and center of gravity are aligned (Shevell 1983); for a slightly irregular elongated hailstone (e.g., egg shaped) the center of gravity would be somewhere along the maximum diameter (Fig. 1). The drag force would exert a torque on this body unless it is falling with the largest diameter vertically oriented. Thus, it appears that both large oblate and elongated hailstones would tend to be vertically oriented.

In situ verification of hydrometeor types and amounts is extremely difficult and in our case was not available. Therefore, we will rely on existing models and self-consistency of data to interpret the forthcoming observations. A simple scattering model assumes a monodispersed distribution of sizes with specified shape, orientation, and dielectric constant to obtain the various polarimetric parameters. Integration over assumed size distributions sometimes leads to better reproduction of observations. Because melting produces significant changes in polarimetric signatures, it is important to accurately model the melting process (Rasmussen and Heymsfield 1987). By combining scattering and melting models, a more realistic interpretation of data might be possible (Bringi et al. 1986). In this paper we use the scattering–melting model of Aydin and Zhao (1990) and the scattering model of Balakrishnan and Zrnić (1990a,b) to help interpret the radar data.

3. Observations

We present samples of data, collected on 6 June 1989 during the Cooperative Oklahoma P-3 Studies Program, to illustrate the diagnostic power of polarization variables. On that day a severe hailstorm was observed by both the WSR-88D radar located in Norman, Oklahoma, and the dual-polarized radar (CIM) located at

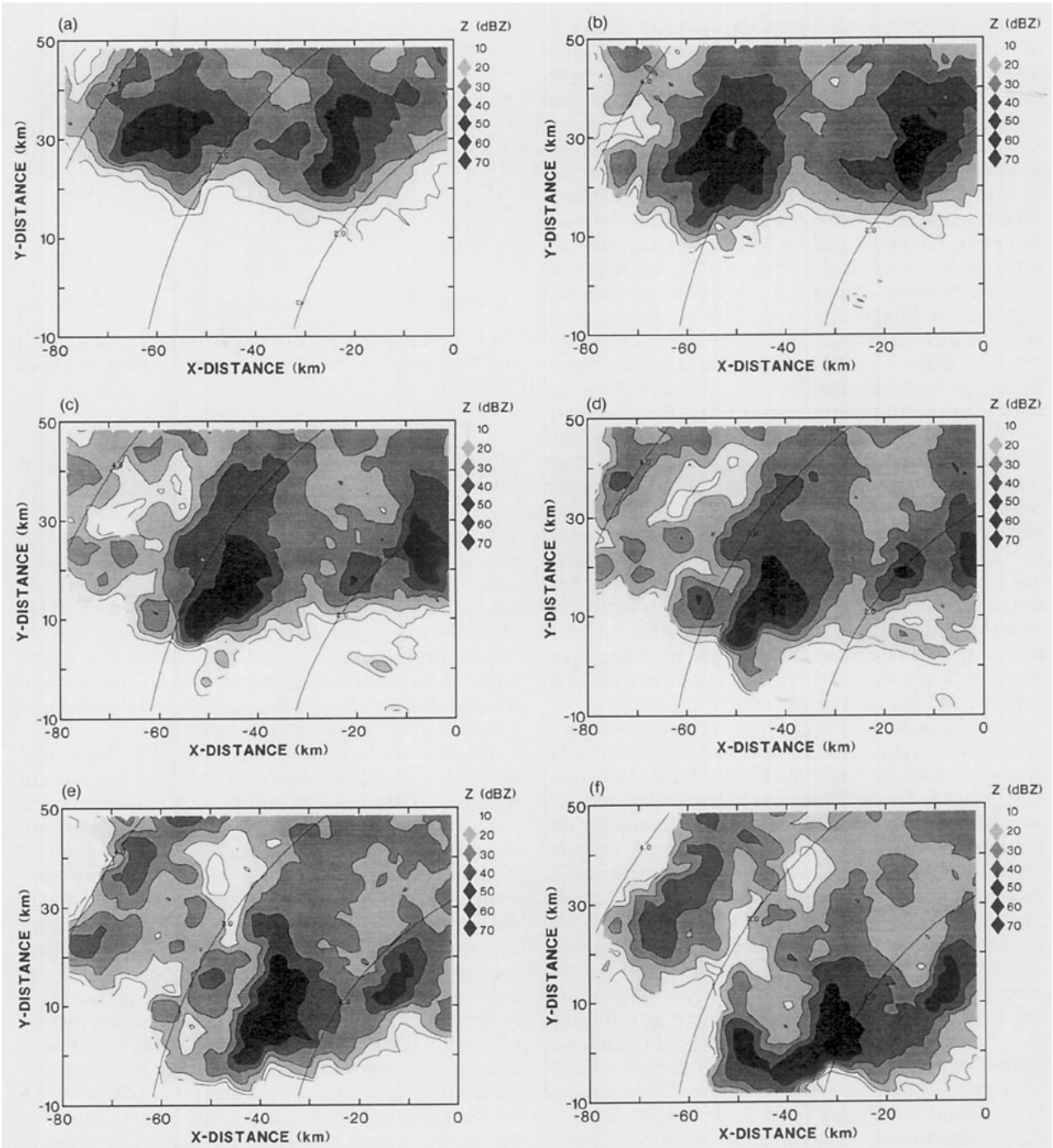

FIG. 2. Reflectivity factor fields at 1.5° elevation from the prototype WSR-88D radar located in Norman. Times are (a) 1404, (b) 1415, (c) 1425, (d) 1430, (e) 1441, and (f) 1451 CST. The origin of the grid is at the location of the Cimarron radar; X and Y are distances west and north of the radar. The circular arcs refer to height above ground. (Their center is at the location of the WSR-88D radar, which is 33 km east and 27.6 km south from the origin.) The reflectivity contours start at 10 dBZ and are spaced 10 dB apart.

Cimarron (40 km and 340° in azimuth from Norman). On the previous day a mesoscale convective system developed in Kansas and left outflow boundaries in western Oklahoma. By midday isolated storms began to develop on the boundary due to moist warm-air advection. Storms moved south-southeastward producing hail up to the size of softballs, and very strong winds. Peak reflectivity measured by the WSR-88D (which transmits right circularly polarized wave and receives left circular) was 70.5 dBZ in the storm of

interest at 1524 CST (central standard time; henceforth, all times are central standard time, which is identical to the local time).

We began scanning the CIM radar and collecting time series data at 1433 CST. The data consisted of 256 complex samples from each resolution volume; the transmitted polarization was alternating between H and V states, and the received state was copolar to the transmit state. The resolution volumes were spaced 300 m apart for the range–height indicator (RHI) scans taken at 1433 and 1500 CST, and 450 m apart for the RHI scan at 1504 CST. These data were processed to yield range profiles of reflectivity [effectively, $(Z_H + Z_V)/2$, denoted as Z from here on] Z_{DR}, ρ_{hv} and ϕ_{DP} using algorithms given by Mueller (1984), Sachidananda and Zrnić (1989), and Balakrishnan and Zrnić (1990b). We filtered ϕ_{DP} in range as suggested by Hubbert et al. (1991, 1992) to estimate K_{DP} and the backscatter differential phase δ. Typical standard errors of measurement are 1 dBZ for Z, 0.2 dB for Z_{DR}, 0.01 for ρ_{hv}, and 3°–5° for ϕ_{DP}. The standard error for δ is estimated to be about 3° (comparable to ϕ_{DP}). The K_{DP} accuracy is difficult to estimate because two types of range filters with different "cutoff wavelengths" (6-dB points being 0.4 and 1.6 km) were used to smooth the ϕ_{DP} range profiles, but we estimate that it is better than 0.3° km^{-1} (Hubbert et al. 1992).

4. Data analysis

In this section data fields from the WSR-88D radar are analyzed to extract general features of the storms, and three RHI cross sections of polarimetric variables are examined in detail.

a. WSR-88D data

Figures 2a–f show a time sequence of conical scans [plan position indicator (PPI)], at 1.5° elevation angle, of reflectivity during the period 1400–1500 CST. Note that the grid origin is located at the CIM radar site. The WSR-88D is at (33, −27.6 km) relative to the origin in Fig. 2, that is, 33 km east and 27.6 km south of the CIM radar site. The storm of interest is centered at (−60, 30) in Fig. 2a. The core moves south-southeastward toward the CIM radar at approximately 40 km h^{-1}. The peak reflectivity of 70.5 dBZ occurred at 1430 CST (Fig. 2d) at a height of 5 km AGL (henceforth, all heights are above ground level). At 1451 CST (Fig. 2f) the reflectivity structure loses its "compactness" and begins to form a squall line.

Lightning struck the Cimarron radar at 1505 CST, and shortly thereafter the line passed over the site. At the site we witnessed high winds and at least two precipitation cells; the first one had intense rain, whereas the second had heavy rain mixed with 25-mm-diameter hail. Note the "shadow" (at −45, 5 km in Fig. 2f) cast by the intense cells to the southeast; this attenuation is primarily caused by depolarization of the circularly polarized wave as it propagates through the intense rain shaft.

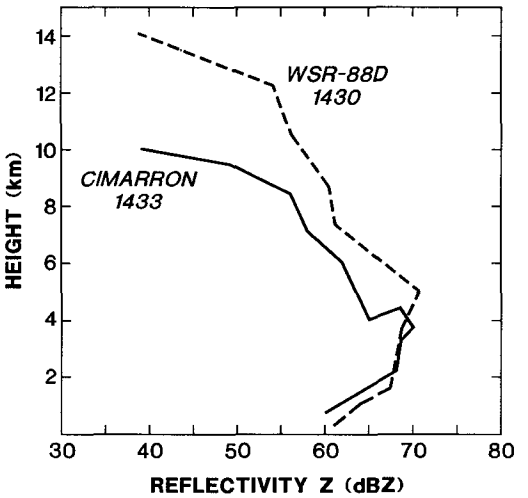

FIG. 3. Vertical profiles of the peak reflectivity factor from Cimarron and WSR-88D radars at about 1430 CST.

Figure 3 shows the plot of peak reflectivity as a function of height at 1430 CST; for comparison, a similar plot of peak reflectivity, estimated as $(Z_H + Z_V)/2$ with the CIM radar at 1433 CST, is also included. Note that the CIM data were obtained from an elevation scan (RHI) centered at (−43.7, 11) in Fig. 2d. Nevertheless, the peak reflectivities from both radars, that is, WSR-88D and CIM, are in good agreement.

Figures 4a–f show the PPI time sequence of mean Doppler velocity v at low elevation angles (0.5° or 1.5°) from WSR-88D in the time interval 1405–1445 CST. Figures 4a–d are at 1.5° elevation angle, whereas Figs. 4e, f are at 0.5°. Between 1405 and 1430 CST, radial convergence is clearly evident in the storm of interest over the height range 2.5–3.5 km. At 1425 CST, radial convergence was observed at 0.5° (not shown here). But, at 1430 CST the 0.5° PPI scan in Fig. 4e depicts a weak radial divergence signature near (−47.5, 12.5), which is slightly northwest of the main reflectivity core in Fig. 2d and is caused by the deflection of precipitation downdraft at the surface. The signature is clearer in Fig. 4f at 1445 CST near (−40, 0). Note, however, that radial convergence with cyclonic rotation is evident on the southeast side of the storm core in both Figs. 4e, f; this is where the leading edge of the gravity current interacts with storm inflow (e.g., Lemon and Doswell 1979; also see Fig. 9.2a in Doviak and Zrnić 1984). The surface-level flow in the environment was from the southeast (2–3 m s^{-1}), while the upper-level flow was from the northwest (12–15 m s^{-1} between 750 and 400 mb), causing the reflectivity structure to appear slanted in vertical sections; for example, see Fig. 5a.

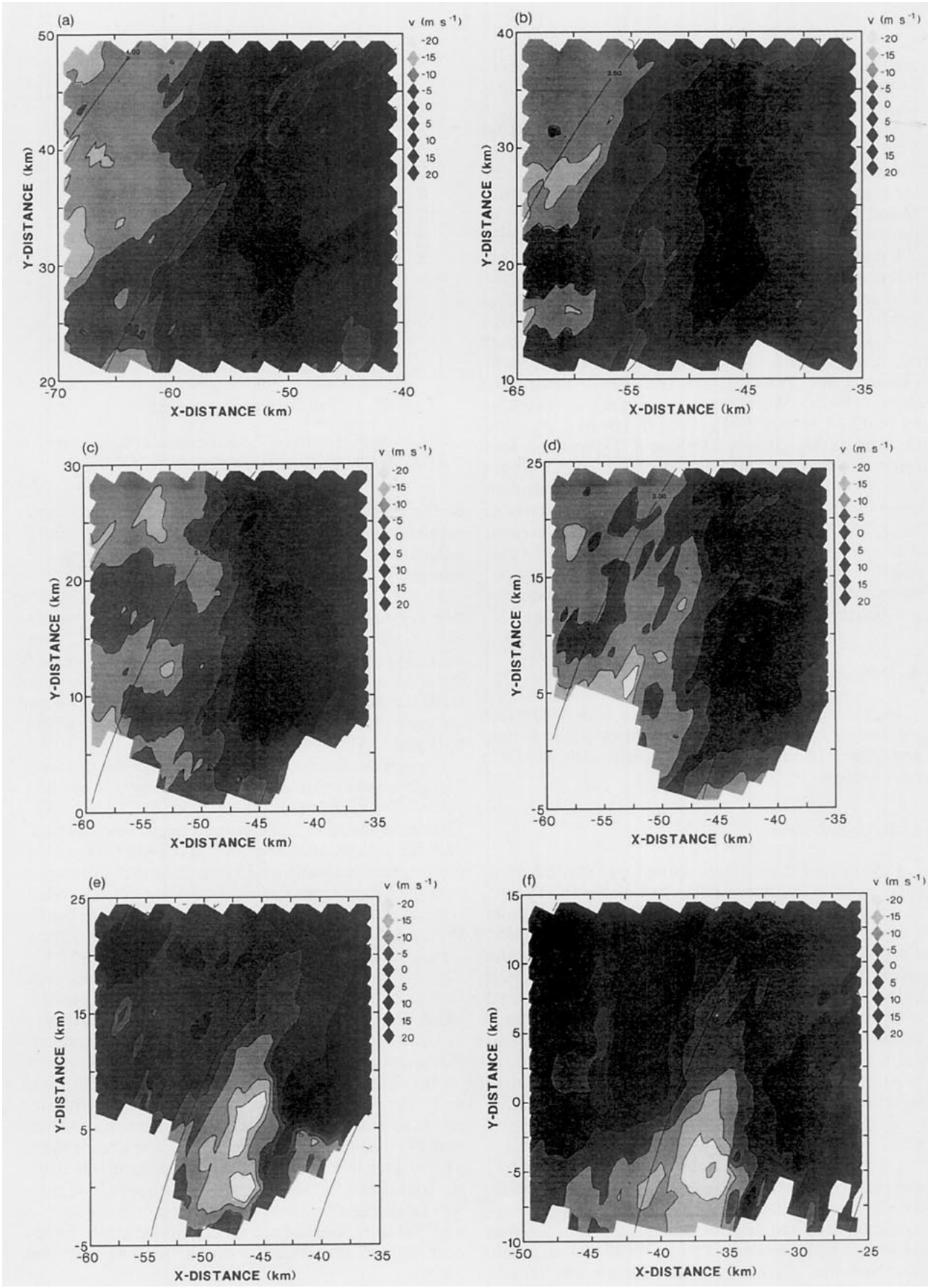
(a)
v (m s⁻¹)
-20
-15
-10
-5
0
5
10
15
20
Y-DISTANCE (km)
X-DISTANCE (km)
(b)
(c)
(d)
(e)
(f)

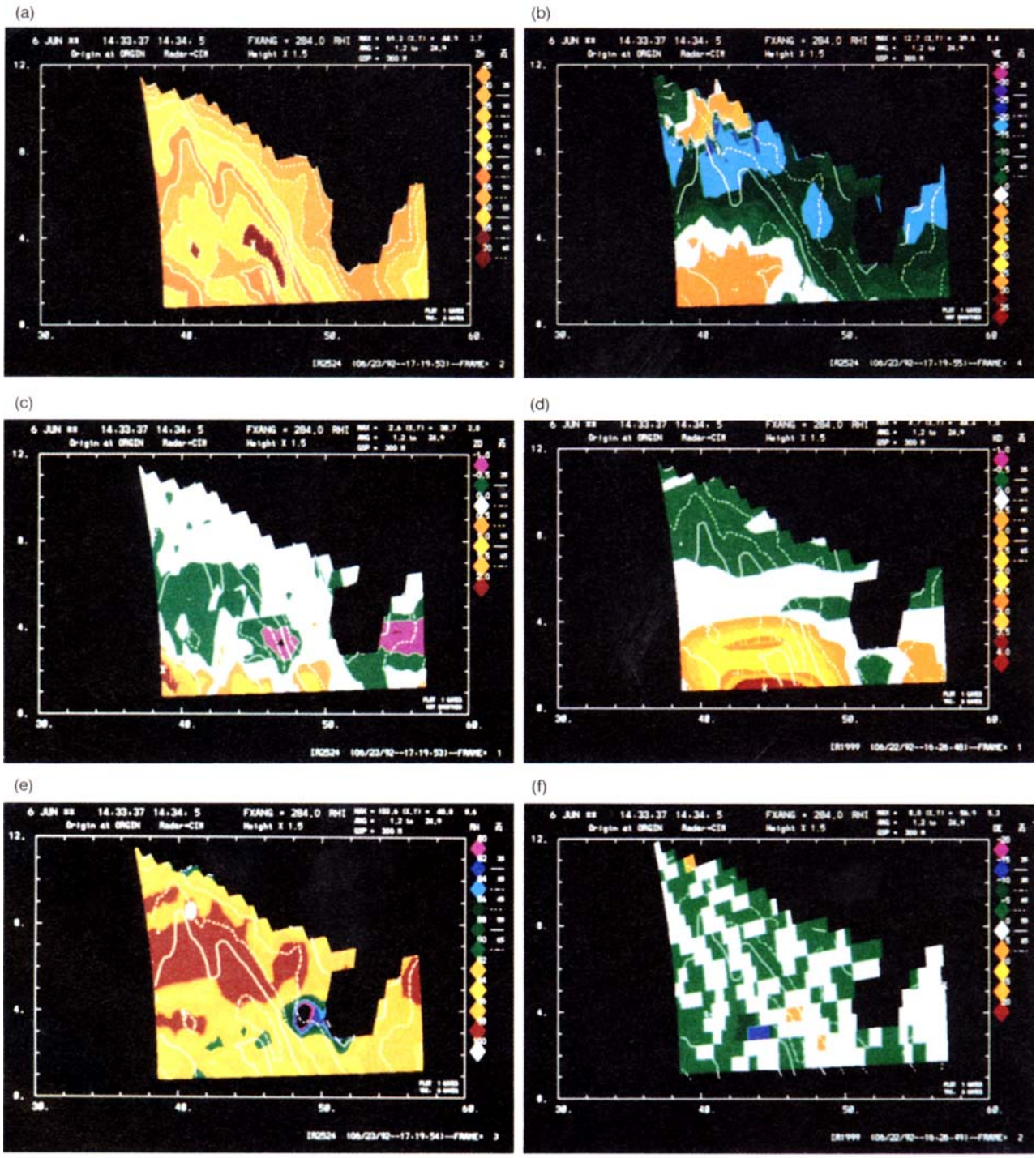

FIG. 5. Range–height cross sections of the (a) reflectivity factor field (dBZ), (b) Doppler velocity field (m s^{-1}), (c) differential reflectivity Z_{DR} (dB), (d) specific differential phase K_{DP} (deg km^{-1}), (e) correlation coefficient ρ_{hv}, and (f) backscatter differential phase δ (deg). The contours are of reflectivity factor starting at 20 dBZ in steps of 10 dB. Range and height are in kilometers. Data are from the Cimarron radar, azimuth angle is 284°, and time is 1433 CST.

FIG. 4. Doppler velocity fields obtained by the WSR-88D radar. Times and elevation angles are (a) 1405 CST and 1.5°, (b) 1415 CST and 1.5°, (c) 1425 CST and 1.5°, (d) 1431 CST and 1.5°, (e) 1430 CST and 0.5°, and (f) 1445 CST and 0.5°. Here X and Y distances are west and north of the Cimarron radar. Velocity contours are in meters per second, and negative values refer to motion toward the WSR-88D radar.

b. CIM polarimetric data at 1433

Figures 5a and 5b show the range–height cross sections of Z and v through the core of the storm cell at 1433 CST. The corresponding cross sections of Z_{DR}, K_{DP}, ρ_{hv}, and δ are in Figs. 5c–f. As mentioned earlier, the RHI scan passes through the point (−43.7, 11) in Fig. 2c.

The reflectivity structure (Fig. 5a) exhibits two tilted cells with maximum $Z > 60$ dBZ. The closer cell, termed cell A1433 (centered at 42 km in range) is at the leading (or southeast) edge of the storm, whereas the farther cell, termed cell B1433 (centered at 45 km), is at the trailing (or northwest) side. Recall from Fig. 4e that a radial divergence signature was noted at 1430 CST slightly northwest of the storm core, while radial convergence was persistent on the southeast side. The radial at the lowest elevation angle (0.3° in Fig. 5b) contains a divergence signature with maximum outbound velocity of 13 m s^{-1} at 50 km in range, and minimum inbound velocity of −10 m s^{-1} at 43 km; the zero velocity is at the surface and centered at 48 km in range below cell B1433. Clear depiction of mid-level radial convergence between the heights of 3–4 km is visible (Fig. 5b); similar observations have been identified as positive precursors of downbursts in Oklahoma (Eilts and Oakland 1989). The maximum inbound velocities reach −15 m s^{-1} at a horizontal distance of 48 km and height between 4 and 5 km in Fig. 5b. This most likely represents entrainment of surrounding air by the precipitation-driven downdraft. The peak Z of 70 dBZ occurs in cell B1433 at a height of 3.6 km and range of 45 km. Near this location, Z_{DR} has its most negative value of −0.8 dB; see Fig. 5c at the horizontal distance of 46–48 km and height of 3.5 km. Negative Z_{DR} values in convective storms have been previously correlated with hail (Bringi et al. 1984; Husson and Pointin 1989). It is significant that the most negative Z_{DR} region is centered on the strongest radial convergence. This suggests that hail loading and melting contributed to downdraft intensification in addition to evaporation and rain loading (Srivastava 1987).

The microphysical origin of the negative Z_{DR} is not known, and there are at least three plausible models that are consistent with this observation. These are 1) vertically oriented cones smaller than about 4 cm (Fig. 1) (Aydin et al. 1984), 2) vertically oriented (largest dimension) oblates less than about 4 cm, and 3) horizontally oriented (largest dimension) oblates bigger than about 4 cm.

Within cell B1433, the maximum K_{DP} is about 3.5° km^{-1} and occurs at a height of 0.9 km and range of 47 km. Using the relation for rain rate, $R = 40.5(K_{DP})^{0.85}$, yields a maximum rain rate of 117 mm h^{-1}, (Chandrasekar et al. 1990). Note that this relation is similar to the one proposed by Sachidananda and Zrnić (1987), who define K_{DP} for a two-way propagation path. At the location of maximum K_{DP} in cell B1433, Z = 60 dBZ, Z_{DR} = 0.5 dB, and ρ_{hv} = 0.95. The Z–Z_{DR} combination indicates presence of hail (Aydin et al. 1986). These values for the precipitation shaft of cell B1433 are consistent with previous observations in Oklahoma storms by Balakrishnan and Zrnić (1990a,b). The radar parameters indicate precipitation composed of raindrops ($R \sim 120$ mm h^{-1}) and, because of very high Z (peak of 70 dBZ) and negative Z_{DR}, large hailstones.

The maximum K_{DP} in Fig. 5d is 4.7° km^{-1} (R = 150 mm h^{-1}) and occurs at a range of 44 km and height of about 1 km and is collocated with the 60-dBZ contour of cell A1433. The sloping (east to west) of the high (>4° km^{-1}) K_{DP} (Fig. 5d) as well as of the reflectivity contours is caused by the shear in environmental wind. In the region of high K_{DP} (>3° km^{-1}) within the main precipitation shaft, the corresponding Z_{DR} is in the range 0.5–1.5 dB. Because these K_{DP} and Z_{DR} values are consistent with the model of Balakrishnan and Zrnić (1990a), we speculate that the surface precipitation shaft contains rain and, possibly, oblate hail with negligible water coating (peak hail rate of 30 mm h^{-1}). The environmental sounding showed the 0°C level at 3.9 km, and we see an increase of K_{DP} to about 0.75° km^{-1} between 3.5 and 4.0 km in height. This indicates formation of raindrops via melting of ice in sufficient concentrations to produce a rain rate of about 30 mm h^{-1}. Note that Z_{DR} in this region is in the range −0.5–0.5 dB possibly due to its well-known sensitivity to the larger, "quasi-spherical" hail particles.

The maximum Z_{DR} of 2.6 dB in Fig. 5c occurs at 2-km height on the southeast (inflow) side of the storm; see also Fig. 4d. In this region of high Z_{DR}, the K_{DP} is very small, implying negligible rain rate; thus, the precipitation in the high-Z_{DR} region might be composed of a low concentration of large raindrops. We do not know the source of such raindrops but offer the following hypothesis from Höller et al. (1991), who observed similar high Z_{DR} values on the inflow side of a hailstorm in Germany. Because the flow within the main precipitation shaft above 4 km is strong northwesterly, it is possible that smaller hailstones are advected farther (since their terminal velocity is smaller) by the horizontal wind; as they melt they produce the larger Z_{DR} values observed on the inflow side.

Figure 5e shows the ρ_{hv} range–height cross section. Balakrishnan and Zrnić (1990b) discuss various factors that can cause ρ_{hv} to decrease from unity. The main factors are a variance in "effective" shapes of the particles with size (accounting for particle canting and dielectric constant variations, e.g., dry versus wet) and variation in δ with size. In both cells A and B, a few values less than 0.92 are visible. In pure rain it was experimentally determined that mean ρ_{hv} was between 0.98 and 0.985 (Balakrishnan and Zrnić 1990b). Transition to lower ρ_{hv} values (less than 0.95 at a height of about 5 km in cell A1433) might indicate a region

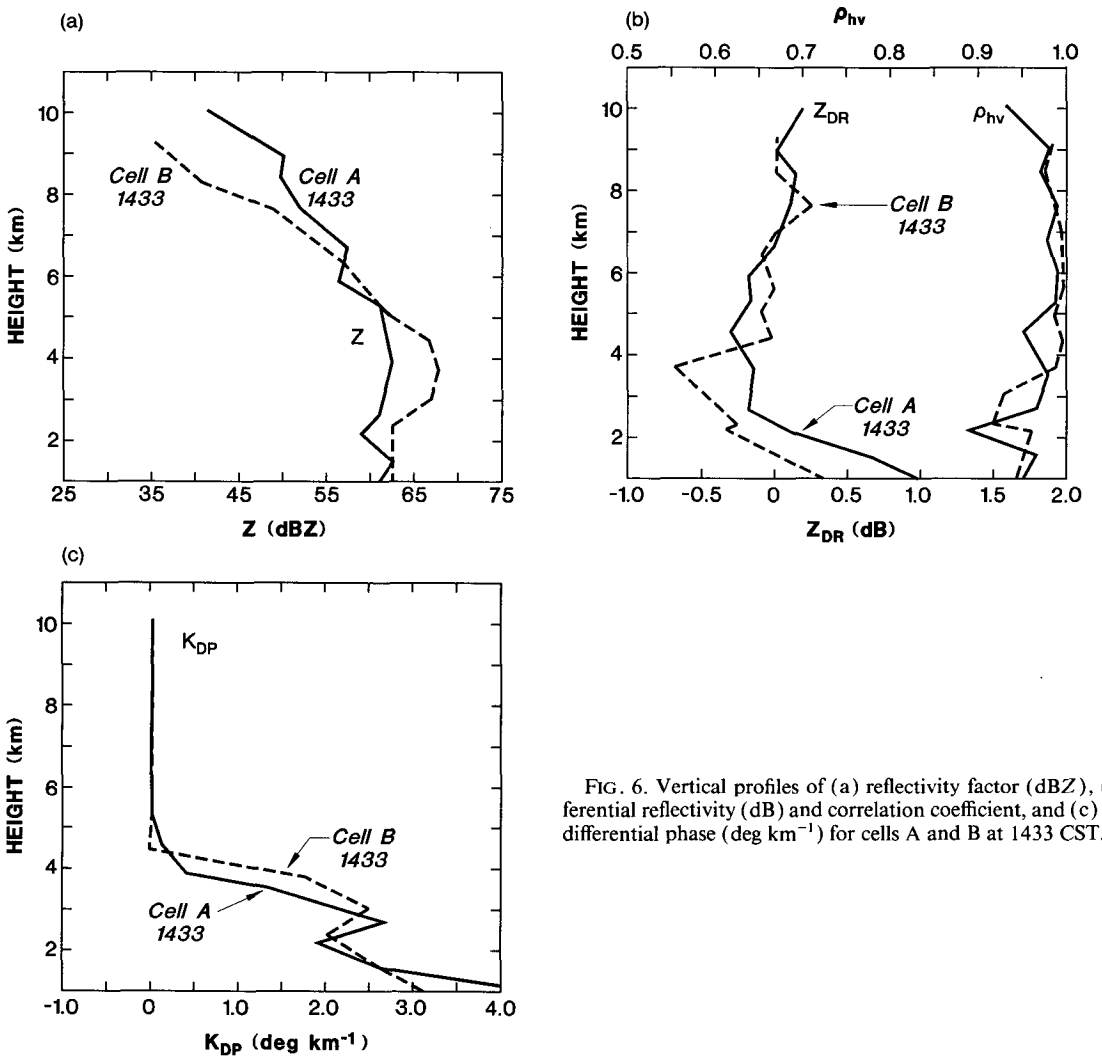

FIG. 6. Vertical profiles of (a) reflectivity factor (dBZ), (b) differential reflectivity (dB) and correlation coefficient, and (c) specific differential phase (deg km^{-1}) for cells A and B at 1433 CST.

where contributions to the water content by ice and liquid hydrometeors are comparable. Also it could be due to large (>1 cm) and wet hydrometeors that produce significant variations in the backscatter differential phase (Zrnić et al. 1992). Both conditions occur after the onset of melting to which, in this case, we attribute this depression in ρ_{hv}. The height of the 0° isotherm in the environmental sounding was at 3.9 km, and the fact that the "bottom of the melting layer" is higher suggests that it was raised by the updraft. Thus, the lower ρ_{hv} values signify hail mixed with rain in agreement with previous data and computations reported by Balakrishnan and Zrnić (1990b). In the trailing core (cell B1433) the ρ_{hv} depression has been lowered to 4 km by the downdraft.

Figure 5f shows the range–height cross section of δ. Experimentally we have determined that in pure rain δ is between ±5° due to statistical uncertainty. Most of the δ values are within the measurement error except for a few points at a height of 3 km and range of 44 km where δ is negative (−10° to −15°). This location is on the edge of cell B1433. We defer further discussion of δ until we consider the next range–height cross-sectional scan taken at 1500 CST.

Figures 6a–c summarize the radar parameters of cell A1433 and cell B1433. The parameters are averaged over a horizontal distance of about 2 km. Because the precipitation shafts were tilted, the data values were estimated along the tilted direction. Cell B (Fig. 6a) has a prominent reflectivity "bulge" between 2.5 and 4.5 km that corresponds to the descent of the precipitation core. Cell A has higher reflectivities above 6 km. Both cells exhibit similar Z_{DR} profiles above 4 km (Fig. 6b). The decrease of Z_{DR} to negative values in cell B coincide with the reflectivity "bulge." Near the surface Z_{DR} is larger in cell A; nevertheless, the Z–Z_{DR} combination for both cells suggests the presence of hail. The vertical profiles of Z_{DR} are consistent with the av-

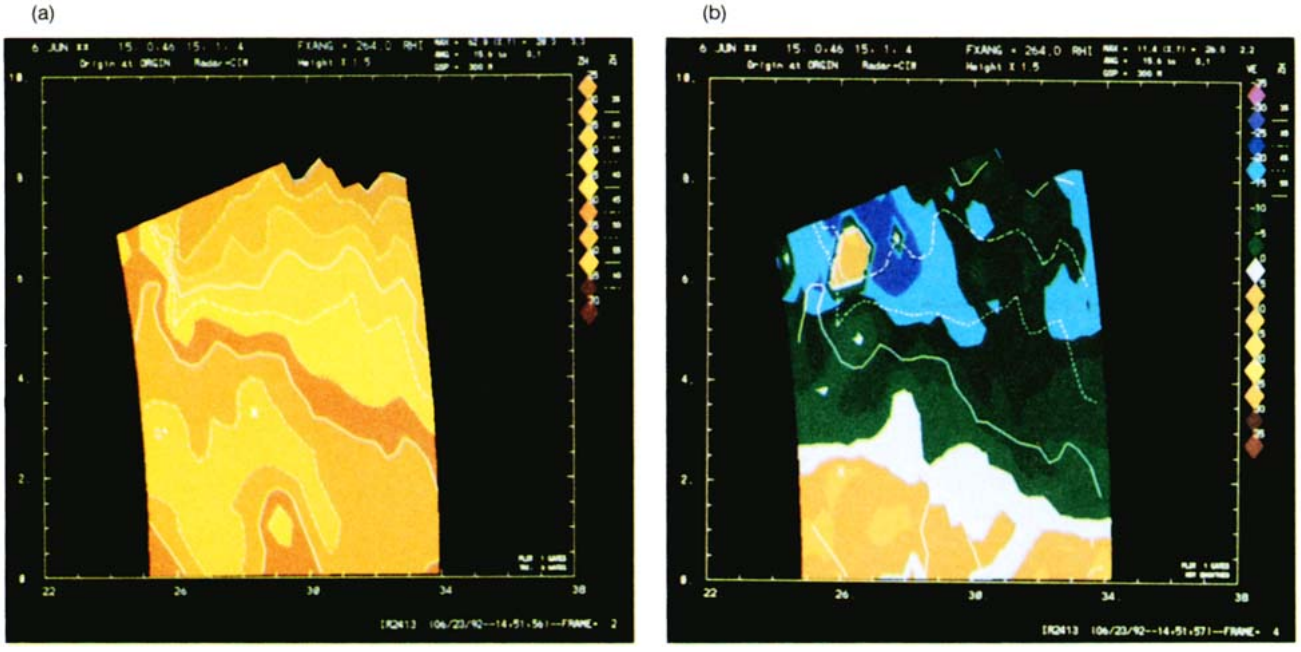

FIG. 7. Same as in Figs. 5a,b except time is 1500 CST and az = 264°.

erage Z_{DR} profiles deduced by Aydin et al. (1989) within the hail regions of a severe hailstorm observed in Denver using the National Center for Atmospheric Research (NCAR) CP-2 radar. They found average Z_{DR} near the surface to be 0.6 dB.

The ρ_{hv} profiles are also compared in Fig. 6b. In cell B above the freezing level ρ_{hv} has a uniformly high value of 0.98. At a height of 3.6 km, which is 300 m below the freezing level, ρ_{hv} decreases. As already explained, this is caused by the variance of "effective" shapes that is largest when liquid and frozen precipitation coexist (i.e., at a height below the onset of melting). The updraft in cell A has raised the height, where ρ_{hv} profile drops below 0.98, to 4.5 km.

Considering K_{DP} profiles (Fig. 6c), note that cell A has larger K_{DP} near the surface. The precipitation "bulge" at 2.5–3 km appears in both cells.

c. *CIM polarimetric data at 1500 CST*

From 1435 to 1500 CST the storm core moved south-southeastward at about 36 km h^{-1}. A range–height scan was obtained through the core. [The location of this scan is defined by the origin and the point (−30, −3) in Fig. 2f.] Figures 7a,b show the cross sections of Z and v; the corresponding cross sections (in color) of Z_{DR}, K_{DP}, ρ_{hv}, and δ are in Figs. 8a–d. The main precipitation shaft can be clearly seen in Fig. 8b with a peak K_{DP} of 4.1° km^{-1} (R = 135 mm h^{-1}, range 31 km). Near the surface (0.5-km height) the parameter values are $Z \sim$ 60–62 dBZ, $Z_{DR} \sim$ 1–2 dB, $K_{DP} \sim$ 3–3.5° km^{-1}, $\rho_{hv} \sim$ 0.92–0.97, and $\delta \sim -10°$ to −15°. We designate this precipitation shaft as cell C1500. The other cell D1500 (at 0.5 km in height, range of 27 km, Fig. 7a) is characterized by parameter values $Z \sim$ 60–62 dBZ, $Z_{DR} \sim$ 0–0.8 dB, K_{DP} = 2.5°–3° km^{-1}, $\rho_{hv} \sim$ 0.86–0.92, and $|\delta| < 5°$, which are quite different from the parameters for cell C1500. The most distinguishing feature of cell D1500 is the band of low ρ_{hv} (0.86–0.92) at heights below 0.5 km and horizontal distance of 26–28 km (Fig. 8c). Other features of cell D1500 are the near-0-dB Z_{DR} below 2 km in height (Fig. 8a) and δ between −5° and 0° (Fig. 8d).

The vertical profiles of ρ_{hv} and K_{DP} below the melting level in cell D1500 are consistent with the Aydin and Zhao (1990) model of melting hail. The model assumes exponential hail size distribution (Cheng and English 1982) and numerically solves melting according to the method of Rasmussen and Heymsfield (1987). A brief description of the Aydin and Zhao model follows. Under steady-state conditions smaller hail particles melt into raindrops. The maximum hail diameter is 50 mm at the 0°C level, and hailstones are oblate in shape but with minor axis in the horizontal plane; such orientations give negative Z_{DR}. We refer to these hydrometeors as vertically oriented (i.e., the long dimension) oblates. A Gaussian canting angle distribution with standard deviation of 45° is used to simulate wobbling. From Fig. 4a (adapted from Aydin and Zhao 1990), we see that ρ_{hv} decreases systematically with decreasing height below the freezing level (5.2 km in the model) provided $\Lambda < 0.6$ mm^{-1}. The corresponding δ (Fig. 9b) is negative and decreases at lower heights.

By comparing Aydin and Zhao model results (Figs. 9a,b and K_{DP} not shown here) with ρ_{hv}, K_{DP}, and δ data, we conclude that the precipitation shaft of cell

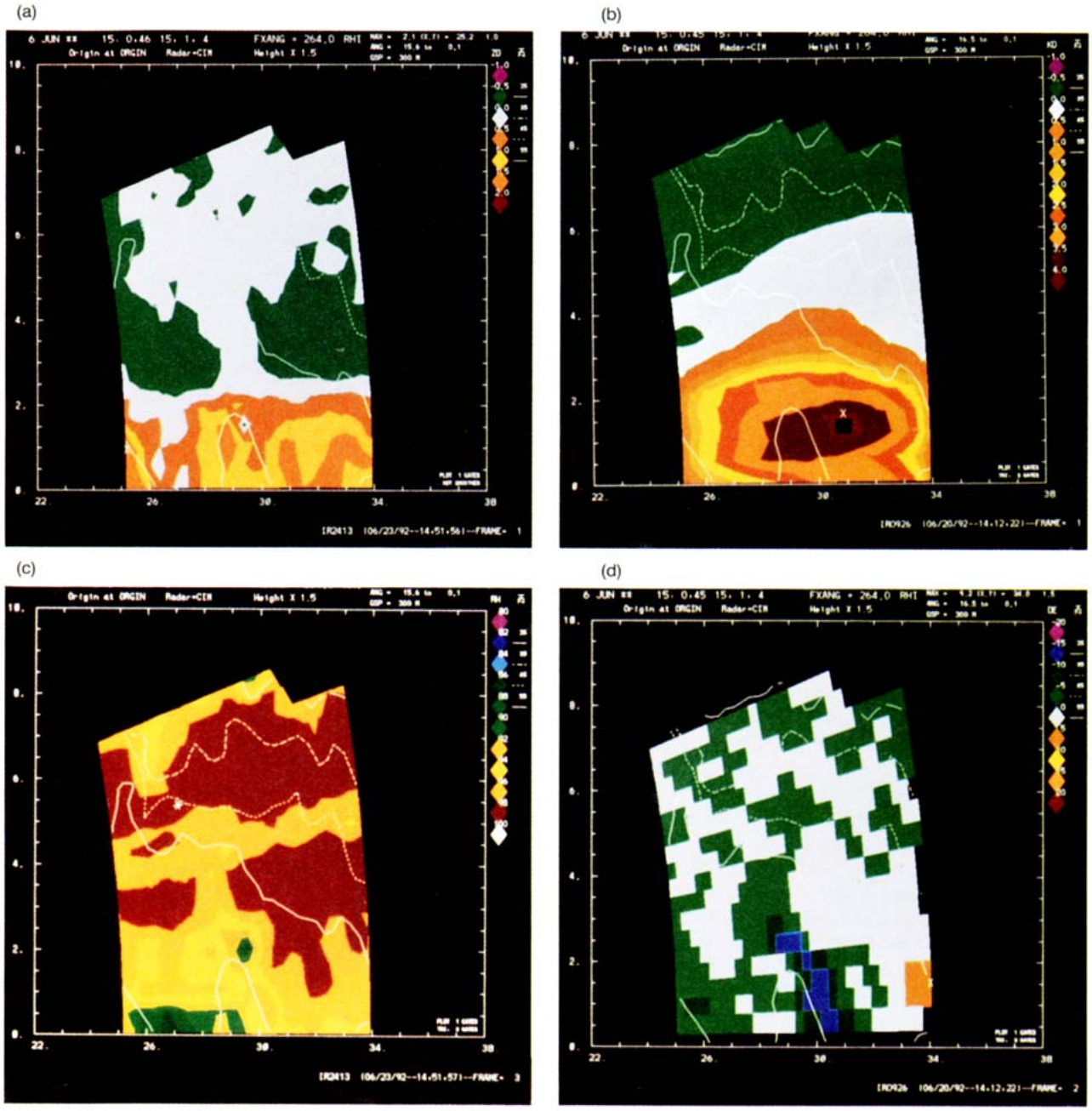

FIG. 8. Same as in Figs. 5c–f except time is 1500 CST and az = 264°.

D1500 might consist of rain (rain rate of 100 mm h^{-1}) mixed with hail ($\Lambda \approx 0.45$–0.35 mm^{-1}, which corresponds to a median volume diameter of approximately 7–8 mm). The concentration N_0 is then between 15 and 60 m^{-3} mm^{-1}. These deduced hail size distribution parameters are within the experimental values considered by Ulbrich and Atlas (1982; see their Fig. 11). The Aydin–Zhao model predicts negative Z_{DR} (−1.5 dB), for $\Lambda < 0.5$ mm^{-1}, because the canting angle model assumes the symmetry axis to be in the horizontal plane and perpendicular to the radar beam. In fact, it is more realistic to assume a random orientation of the symmetry axis in the horizontal plane (Vivekanandan et al. 1991); this would cause both Z_{DR} and δ to be in closer agreement with the measured value of nearly 0 dB and 0°. The Aydin–Zhao model also gives reflectivity about 10 dBZ higher than observed, which can be accounted for by a reduction in the maximum hailstone diameter D_{max} (assumed as 50 mm in the model).

Considering cell C1500, the distinguishing features are the high K_{DP} values (3–4° km^{-1}, Fig. 8b) correlated

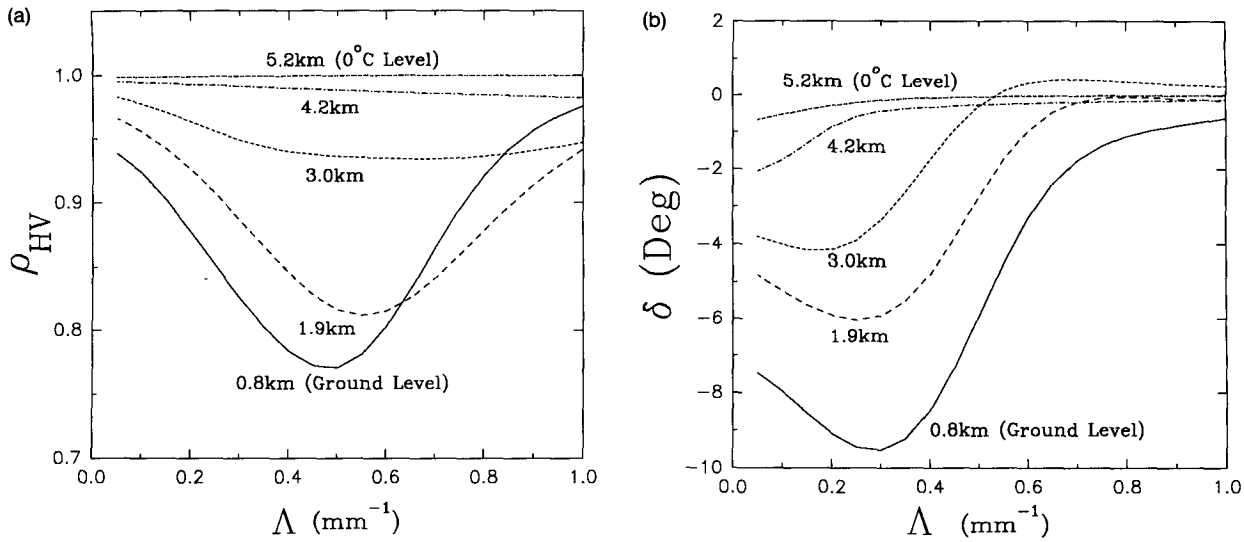

FIG. 9. (a) Correlation coefficient versus the slope Λ of the Cheng–English (1983) hail size distribution. The 0° level is at 5.2 km, and the heights below it are indicated (from Aydin and Zhao 1990 model). (b) Same as in (a) except δ is plotted.

with the 60-dBZ contour, as well as the shaft of negative δ ($-10°$ to $-15°$) in Fig. 8d. A minimum in ρ_{hv} ($\sim$0.86) is visible at a height of 2 km (Fig. 8c). Below 2 km, the Z_{DR} values are higher than in cell D1500, reaching 1.5 dB. Figure 7b shows a region of radial convergence (between 2 and 4 km) centered on cell C, which is dominated by inbound velocities from the west. Entrainment of air by the intense precipitation downdraft (the peak R = 135 mm h^{-1} is deduced from K_{DP} = 4.1° km^{-1}) caused this convergence. The persistent negative δ feature suggests a narrower hail size distribution than deduced for cell D. This will be demonstrated using the δ versus D calculation (Fig. 10), which is valid for horizontally oriented water-coated oblates; such orientation is chosen because the measured Z_{DR} is positive (Fig. 8a) with peaks of about 2 dB. It can be seen (Fig. 10) that negative δ occurs between $8 < D < \sim 16$ mm. Integration of a wide size distribution (e.g., as done for Fig. 9) would produce positive δ (0°–10°), which is contrary to the measurements (cell C1500 in Fig. 8d). To explain the persistent δ between $-10°$ and $-15°$, a narrower size distribution must be invoked. Thus, there appears to be a preferred concentration near sizes (8–16 mm) that give δ between $-10°$ and $-15°$. It is not possible to estimate more precisely the sizes, because they depend on axis ratio of the hydrometeors as well as their dielectric constant (which because of likely wetness would be close to that of liquid water). The few values of negative δ in Fig. 5f (cell B1433) can also be interpreted in this manner.

A local minimum in ρ_{hv} at 2-km height within cell C is observed in Fig. 8c, with higher values above and below. Such a behavior is in accord with the model results in Fig. 9a for Λ larger than 0.65 mm^{-1}, which implies a narrower breadth of the exponential distribution (i.e., hailstone's D_{max} < about 16 mm). It is likely due to the rain reflectivity Z_r becoming comparable to hail reflectivity Z_h as hailstones are melting on descent (Balakrishnan and Zrnić 1990b). In the data given here, at 2-km height, the $Z_r \approx$ 54.8 dBZ and $Z_h \approx$ 55.1 dBZ. The Z_r is obtained from a rain rate of 100 mm h^{-1} (K_{DP} = 3° km^{-1} within cell C at 2-km height) using $Z_r = 400R^{1.4}$ for thunderstorm rain, whereas $Z_h = Z - Z_r$ (mm^6 m^{-3}) and the measured Z = 58 dBZ. Above 2-km height the reflectivity is dominated by hail ($Z_{DR} \approx$ 0 dB), which accounts for the increase in ρ_{hv} ($\sim$0.98). Below 2 km, the increasing rain rate (peak of 135 mm h^{-1}) causes ρ_{hv} to increase.

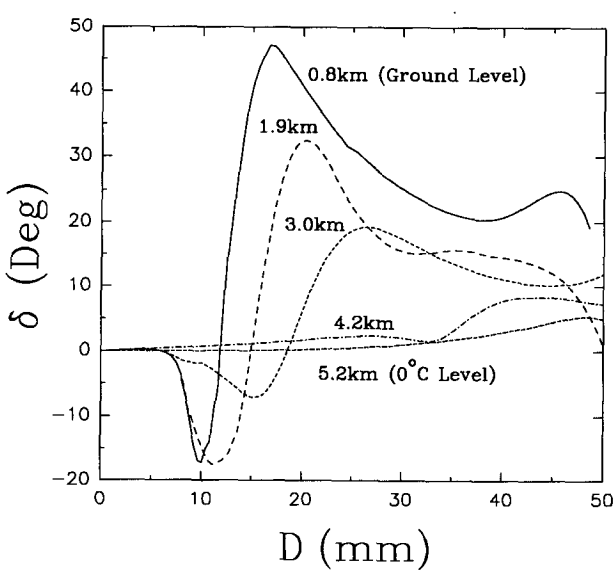

FIG. 10. Backscatter differential phase versus the equivalent spherical diameter of oblate (horizontally oriented) hailstones.

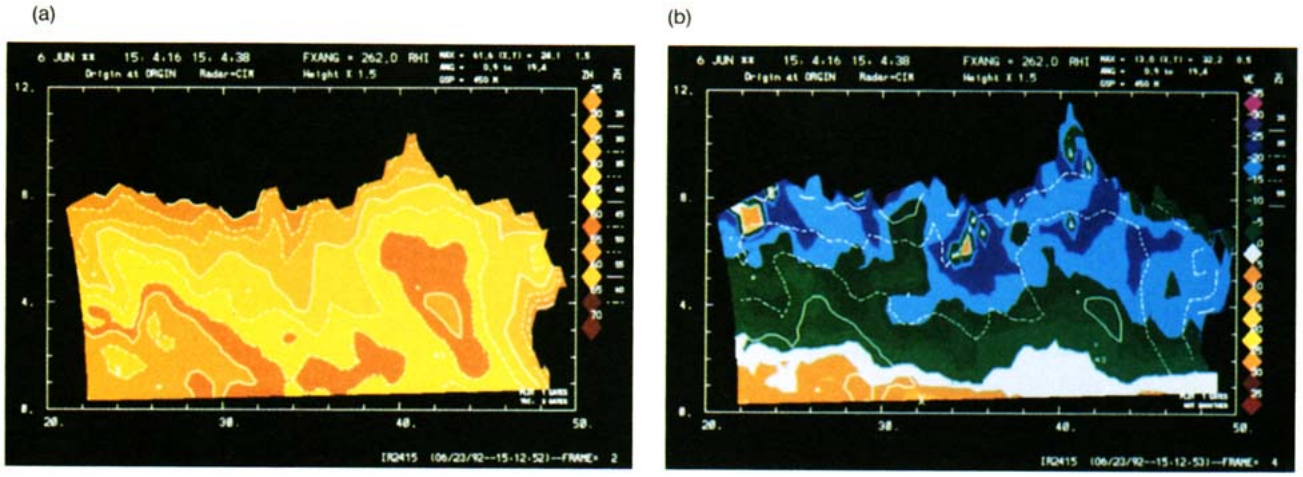

FIG. 11. Same as in Figs. 5a,b except time is 1504 CST and az = 264°.

d. CIM polarimetric data at 1504 CST

At 1504 CST a range–height scan was centered at (−35, −5) in Fig. 2f, and the corresponding radar parameters are in Figs. 11 and 12. The main precipitation shaft at range 27 km has a peak K_{DP} of 4.1° km^{-1} (Fig. 12b). This cell (C1504) is the same as the cell C1500, but the observation is made later and is displaced by 2° in azimuth. Thus, we have a second "snapshot" of cell C about 4 min later, and we note that the K_{DP} structures at the two times are very similar. The main

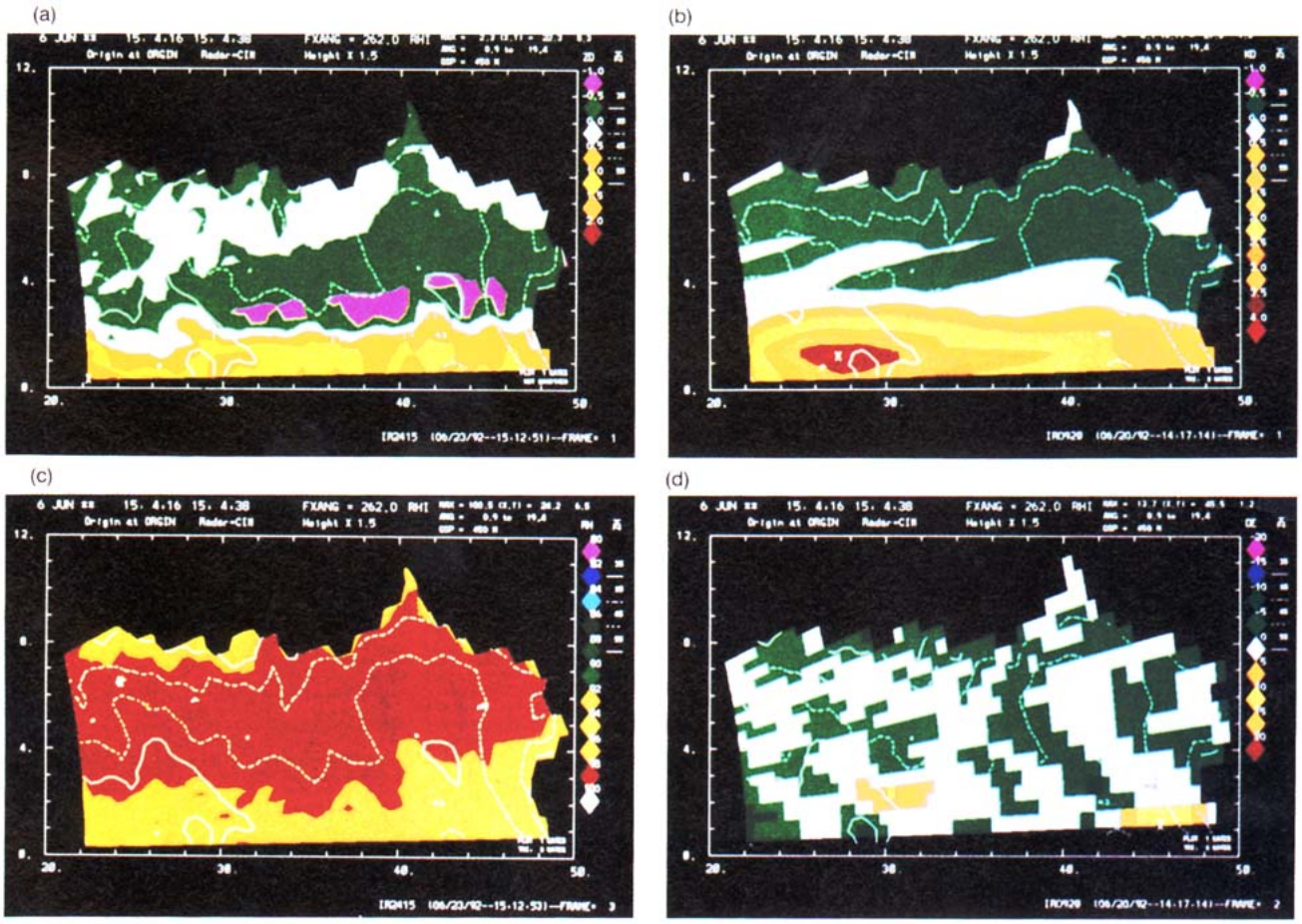

FIG. 12. Same as in Figs. 5c–f except the time is 1504 CST and az = 262°.

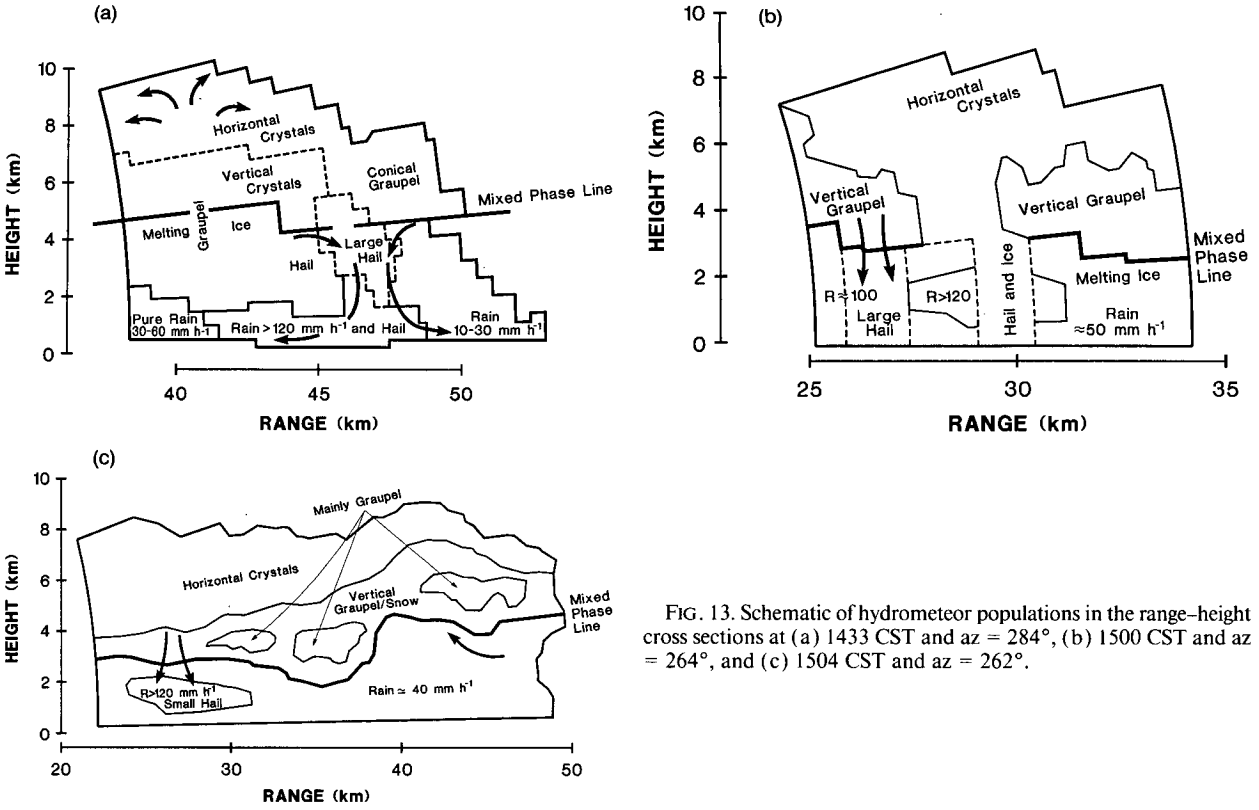

FIG. 13. Schematic of hydrometeor populations in the range–height cross sections at (a) 1433 CST and az = 284°, (b) 1500 CST and az = 264°, and (c) 1504 CST and az = 262°.

difference is in the δ profile at the later time (Fig. 12d), which has most values within ±5°. The persistent negative δ feature noted earlier in cell C1500 (Fig. 8d) has disappeared. (Either the shaft has descended or it is out of the scan plane.) The vertical cross section of the ρ_{hv} field within cell C (Fig. 12c) has a distinct transition at 2.5-km height; the values below are in the range 0.96–0.98, while above they are greater than 0.98. This is quite a change from the earlier profiles (Fig. 8c and 5e). It appears that the cell C1504 is in a decaying stage; a precipitation downdraft now prevails, and it has lowered the melting layer by a kilometer. The 60-dBZ contour has shrunk considerably in vertical extent compared to cell C1500, and the uniformly high ρ_{hv} above 2.5 km suggests that the "effective" ice shapes are more uniform. Near the surface (within cell C1504) the Z_{DR}, Z pair (1–1.5 dB, 55 dBZ) reveals presence of hail. At the location of peak K_{DP} (1.5-km height) the Z = 60 dBZ. As discussed earlier, we estimate $Z_r \approx 55.7$ dBZ and $Z_h \approx 58$ dBZ; this mixture of rain and hail causes a decrease in ρ_{hv} (to 0.97) from that experimentally found for pure rain (0.985). Note Z_{DR} is in the range 0–0.5 dB at this location.

Another cell (E1504) can be identified in Fig. 11a, at the range of 45 km where the 50-dBZ contour rises to 6.5 km in height. The K_{DP} values within this cell (Fig. 12b) are much smaller (1.5°–2° km^{-1}), indicating lower rain rates than in cell C1504. The ρ_{hv} values (Fig. 12c) are uniformly high (>0.98) above 4 km but decrease below; thus, the bottom of the melting zone has not yet been lowered (as in the C cell), probably because cell E has not reached the dissipative stage. This speculation is also consistent with the v profile in Fig. 11b, which exhibits convergence near ground and strong inbound velocities (~ -18 m s^{-1}) on the far side between 3 and 4 km in height (in general agreement with Figs. 5b and 7b). The Z_{DR} cross section (Fig. 12a) has a coherent region of negative values (−0.5 to −1 dB) extending from 30 to 46 km in range and 3–4 km in height. This might be due to vertically oriented conical graupel (similar to the sketch in Fig. 1), which is often found in regions of lower Z (45–55 dBZ). We have verified, by examining the differential phase, that differential attenuation is negligible and thus could not have caused the negative values of differential reflectivity.

From the analysis of the polarimetric data and the mean Doppler velocities it is possible to partition the observed range–height cross sections into regions where certain types of hydrometeors dominate (Fig. 13). The mixed-phase line was drawn at a height where there is a marked decrease of ρ_{hv} (below 0.98) caused by about equal contributions of ice and liquid to the total water mass. We are more confident in the classifications below the freezing level than above it. There, the values of K_{DP} and Z_{DR} are pronounced and considerably larger

than the uncertainty in the estimates; thus, rain rate can be quantified (from K_{DP}); furthermore, rain–hail mixtures can be identified and even quantified using simple models. Above the freezing level slightly negative Z_{DR} (0 to −0.5 dB) is associated with vertically oriented graupel. Near the top of the storms slightly positive Z_{DR} is attributed to horizontally oriented ice crystals.

5. Conclusions

Data samples of polarimetric measurands from a hailstorm at a range of about 40 km have been presented. The data were obtained with the NSSL's 10-cm-wavelength polarimetric radar. The S band has significant operational ramifications because the new WSR-88D weather radars have the same wavelength. Thus, there is a possibility that some of these may be modified to include dual polarization. Even if this does not occur, research findings from polarimetric radars may help interpretation of signatures in the fields of Doppler spectral moments of the nonpolarimetric WSR-88Ds.

Our measurements are the first with good spatial resolution of five polarimetric variables: reflectivity factor, differential reflectivity, specific differential phase, backscatter differential phase, and the correlation coefficient between horizontally and vertically polarized echoes. At present, interpretation of the measurements is possible only for a limited subset of the data and it relies on scattering models and self-consistency of the measurands.

This storm case was also observed with the WSR-88D radar for a period of 1 h. These radar data indicate that the storm (during polarimetric data collection) was severe. Surface divergence signatures were evident in the velocity field, and so were inflow and convergence at the leading edge of the gravity current.

Polarimetric data were collected at the time of peak reflectivity, which was 70 dBZ at 5 km AGL, and a few minutes after the surface divergence was detected. We have made an attempt to identify regions with dominant hydrometeor types and to quantify the amounts of precipitation. Heavy rain shafts have been clearly identified from significant K_{DP} values that also provided quantitative estimates of rainfall in regions of rain mixed with hail. Use of a hail melting model allowed us to estimate the dominant sizes and the breadth of the distribution. We have observed a vertically continuous shaft of negative backscatter differential phase that we attribute to a narrow range of hail sizes (8–16 mm). We do not have independent in situ data aloft for verification, yet self-consistency of polarimetric variables and general agreement with models suggest that our interpretation is plausible.

Acknowledgments. During this study Dr. Balakrishnan was supported by the National Severe Storms Laboratory through a grant to the Cooperative Institute for Mesoscale Meteorological Studies. Participation in data collection by Dr. Aydin was supported by the Army Research Office under Contract DAAL 03-89-K-0158 and the National Science Foundation under Grant ATM-8921014. Drs. Bringi, Chandrasekar, and Hubbert were supported by the U.S. Army Research office through the Center for Geosciences at Colorado State University. Valuable information concerning the meteorological situation was provided by D. Burgess, who also gave advice concerning data interpretation. Mike Schmidt operated the radar during data collection, Yosepha Gal-Chen helped with various aspects of computer manipulations, and Joan Kimpel prepared several figures. Mike Eilts's suggestions improved the clarity of presentation. The authors thank Mr. J. D. Tuttle of NCAR for computing assistance. Computer resources for processing the radar data were provided by NCAR's Scientific Computing Division. Part of this work has resulted from continuing support by the Joint System Program Office of the NEXRAD, which also provided the WSR-88D data.

REFERENCES

Aydin, K., and Y. Zhao, 1990: A computational study of polarimetric radar observables in hail. *IEEE Trans. Geosci. Remote Sens.*, **28**, 412–421.

——, T. A. Seliga, and V. N. Bringi, 1984: Differential radar scattering properties of model hail and mixed phase hydrometeors. *Radio Sci.*, **19**, 58–66.

——, ——, and V. Balaji, 1986: Remote sensing of hail with a dual linear polarization radar. *J. Climate Appl. Meteor.*, **25**, 1475–1484.

——, Y. Zhao, and T. A. Seliga, 1990a: A differential reflectivity radar hail measurement technique: Observations during the Denver hailstorm of 13 June 1984. *J. Atmos. Oceanic Technol.*, **7**, 104–113.

——, Y. M. Lure, and T. A. Seliga, 1990b: Polarimetric radar measurements of rainfall compare with ground-based rain gauges during MAYPOL'84. *IEEE Trans. Geosci. Remote Sens.*, **28**, 443–449.

Balakrishnan, N., and D. S. Zrnić, 1990a: Estimation of rain and hail rates in mixed-phase precipitation. *J. Atmos. Sci.*, **47**, 565–583.

——, and ——, 1990b: Use of polarization to characterize precipitation and discriminate large hail. *J. Atmos. Sci.*, **47**, 1525–1540.

Bringi, V. N., and A. Hendry, 1990: Technology of polarization diversity radars for meteorology. *Radar in Meteorology*, D. Atlas, Ed., Amer. Meteor. Soc., 153–190.

——, T. A. Seliga, and K. Aydin, 1984: Hail detection using a differential reflectivity radar. *Science*, **225**, 1145–1147.

——, R. M. Rasmussen, and J. Vivekanandan, 1986a: Multiparameter radar measurements in Colorado convective storms. Part I: Graupel melting studies. *J. Atmos. Sci.*, **43**, 2545–2563.

——, J. Vivekanandan, and J. D. Tuttle, 1986b: Multiparameter radar measurements in Colorado convective storms. Part II: Hail detection studies. *J. Atmos. Sci.*, **43**, 2564–2577.

Cheng, L., and M. English, 1983: A relationship between hailstone concentration and size. *J. Atmos. Sci.*, **40**, 204–213.

Chandrasekar, V., V. N. Bringi, N. Balakrishnan, and D. S. Zrnić, 1990: Error structure of multiparameter radar and surface measurements of rainfall. Part III: Specific differential phase. *J. Atmos. Oceanic Technol.*, **7**, 621–629.

Doviak, R. J., and D. S. Zrnić, 1984: *Doppler Radar and Weather Observations.* Academic Press, 458 pp.

Eilts, M. D., and S. K. Oakland, 1989: Convergence aloft as a precursor to microbursts. Preprints, *24th Radar Meteorology Conf.,* Tallahassee, FL, Amer. Meteor. Soc., 190–193.

Höller, H., P. F. Meischner, V. N. Bringi, and J. Hubbert, 1991: Hailstorm observations by multiparameter radar. Preprints, *25th Int. Conf. Radar Meteorology,* Paris, Amer. Meteor. Soc., 713–716.

Hubbert, J., V. Chandrasekar, V. N. Bringi, and P. Meischner, 1991: Processing and interpretation of dual-polarized phase measurements. Preprints, *25th Int. Conf. Radar Meteorology,* Paris, Amer. Meteor. Soc., 654–657.

——, ——, ——, and ——, 1993: Processing and interpretation of coherent dual-polarized radar measurements. *J. Atmos. Oceanic Technol.,* **10,** 155–164.

Husson, D., and Y. Pointin, 1989: Quantitative estimation of the hail fall intensity with a dual polarization radar and a hailpad network. Preprints, *24th Conf. Radar Meteorology,* Tallahassee, FL, Amer. Meteor. Soc., 318–321.

Illingworth, A. J., J. W. F. Goddard, and S. M. Cherry, 1987: Polarization radar studies of precipitation development in convective storms. *Quart. J. Roy. Meteor. Soc.,* **113,** 469–489.

Knight, N. C., 1986: Hailstone shape factor and its relation to radar interpretation of hail. *J. Climate Appl. Meteor.,* **25,** 1956–1958.

Kry, P. R., and R. List, 1974: Angular motions of freely falling spheroidal hailstone models. *The Physics of Fluids,* **17,** 1093–1102.

Lemon, L. R., and Doswell, C. A., III, 1979: Severe thunderstorm evolution and mesocyclone structure as related to tornadogenesis. *Mon. Wea. Rev.,* **107,** 1184–1197.

Lipshutz, R. C., J. F. Pratte, and J. R. Smart, 1986: An operational Z_{DR}-based precipitation type/intensity product. Preprints, *23rd Conf. on Radar Meteorology,* Snowmass, CO, Amer. Meteor. Soc., JP91–JP94.

List, R., 1985: Properties and growth of hailstones. *Thunderstorm Dynamics and Morphology,* E. Kessler, Ed., University of Oklahoma Press, 259–276.

Longtin, D. R., and others, 1987: Radar backscattering by large, spongy ice oblate spheroids. *J. Atmos. Oceanic Technol.,* **4,** 355–358.

Mueller, E. A., 1984: Calculation procedure for differential propagation phase shift. Preprints, *22nd Conf. on Radar Meteorology,* Zurich, Amer. Meteor. Soc., 397–399.

Rasmussen, R. M., and A. J. Heymsfield, 1987: Melting and shedding of graupel and hail. Part I: Model physics. *J. Atmos. Sci.,* **44,** 2754–2763.

Sachidananda, M., and D. S. Zrnić, 1987: Rain rate estimates from differential polarization measurements. *J. Atmos. Oceanic Technol.,* **4,** 588–598.

——, and ——, 1989: Efficient processing of alternately polarized radar signals. *J. Atmos. Oceanic Technol.,* **6,** 173–181.

Seliga, T. A., and V. N. Bringi, 1976: Potential use of radar reflectivity measurements at orthogonal polarizations for measuring precipitation. *J. Appl. Meteor.,* **15,** 69–76.

——, and ——, 1978: Differential reflectivity and differential phase shift: Applications in radar meteorology. *Radio Sci.,* **13,** 271–275.

Shevell, R. S., 1983: *Fundamentals of Flight.* Prentice-Hall Inc., 405 pp.

Srivastava, R. C., 1987: A model of intense downdrafts driven by the melting and evaporation of precipitation. *J. Atmos. Sci.,* **44,** 1752–1773.

Steinhorn, I., and D. S. Zrnić, 1988: Potential uses of differential propagation phase constant to estimate raindrop and hailstone size distributions. *IEEE Trans. Geosci. Remote Sens.,* **26,** 639–648.

Ulbrich, C. W., and D. Atlas, 1982: Hail parameter relations: A comprehensive digest. *J. Appl. Meteorol.,* **21,** 22–43.

——, and ——, 1984: Assessment of the contribution of differential polarization to improved rainfall measurements. *Radio Sci.,* **19,** 49–57.

Vivekanandan, J., W. M. Adams, and V. N. Bringi, 1991: Rigorous approach to polarimetric radar modeling of hydrometeor orientation distributions. *J. Appl. Meteor.,* **30,** 1053–1063.

Wakimoto, R. M., and V. N. Bringi, 1988: Dual-polarization observations of microbursts associated with intense convection: the 20 July storm during the MIST project. *Mon. Wea. Rev.,* **110,** 1521–1539.

Zrnić, D. S., N. Balakrishnan, C. L. Ziegler, V. N. Bringi, K. Aydin, and T. Matejka, 1992: Polarimetric signatures in the stratiform region of a mesoscale convective system. *J. Appl. Meteor.,* **32,** 678–693.